Measurement of Interfacial Charge-Transfer Rate Constants at n-Type InP/CH_3OH Junctions

Katherine E. Pomykal and Nathan S. Lewis*

Division of Chemistry and Chemical Engineering, California Institute of Technology, Pasadena, California 91125

Received: August 20, 1996; In Final Form: November 12, 1996[⊗]

Steady-state current density vs potential methods have been used to measure interfacial electron-transfer rate constants at n-type indium phosphide/liquid junctions. n-InP/CH_3OH-1,1′-dimethylferrocene$^{+/0}$, n-InP/CH_3OH-ferrocene$^{+/0}$, n-InP/CH_3OH-tetrahydrofuran-decamethylferrocene$^{+/0}$, and n-InP/CH_3OH-1,1′-diphenyl-4,4′-dipyridinium$^{2+/+\bullet}$ contacts displayed bimolecular kinetic behavior in which the observed current density was first order in the concentration of electrons at the semiconductor surface and in the concentration of acceptors in the solution. Differential capacitance potential measurements were used to determine the energetics for the charge-transfer process as well as to determine the concentration of electrons at the semiconductor surface as a function of applied potential. These measurements indicated that the voltage dropped across the semiconductor space charge region varied linearly with changes in the Nernst potential of the solution, as expected for an ideally behaving semiconductor/liquid junction. The measured charge-transfer rate constants, k_{et}, for these systems were $\approx 10^{-16}$ cm^4 s^{-1}, in excellent agreement with previous theoretical predictions.

I. Introduction

Interfacial charge-transfer rate constants across semiconductor/liquid contacts have recently received a great deal of attention both theoretically and experimentally.[1−10] The factors that control these rate constants comprise some of the most fundamental, yet least understood, aspects of photoelectrochemical energy conversion devices. Very rapid reversible majority carrier transfer is undesirable for photoelectrochemical devices, since rapid collection of majority carriers by acceptors in the solution would result in significant recombination of charge carriers and would thus limit the efficiencies of photoelectrochemical energy conversion devices. However, very slow charge capture of minority carriers is undesirable because it would produce a large overpotential for collection of charge and would result in wasteful voltage losses in the cell. An understanding of the factors that affect interfacial charge-transport processes should also allow design of systems that kinetically direct charge carriers in the solid to react with the desired redox molecules in the solution, thereby improving electrode stability and decreasing deleterious electrode passivation or corrosion reactions.

In this work, we report experimental measurements of interfacial charge-transfer rate constants for n-type InP electrodes in contact with a series of one-electron, outer-sphere redox reagents. These reagents have been chosen because they allow variation in the driving force for the interfacial charge-transfer process while controlling variation in other solvent-related reorganization parameters. In addition, many of these redox couples have been used in efficient InP-based photoelectrochemical cells,[11−13] so understanding the factors that control the interfacial rates at these contacts provides a direct understanding of the factors that control the efficiency losses in such photoelectrochemical energy conversion devices.

The use of outer-sphere redox couples facilitates comparison between experimental rate constant measurements and theoretical predictions. The rate constant, k_{et}, for transfer of an electron in a semiconductor to an outer-sphere redox species in the solution phase can be expressed as $k_{et} = \nu_n \kappa_n \kappa_{el}$,[3,14] where ν_n is the relevant vibrational frequency along the reaction coordinate for the charge transfer event, κ_n is the nuclear term describing the Franck−Condon factors of the reaction, and κ_{el} accounts for the electronic coupling between the reactants. Expressions for κ_n are well-known[3,15−17] and are of the form

$$\kappa_n = e^{-[(\Delta G^{\circ\prime}+\lambda)^2/(4\lambda kT)]} \quad (1)$$

where $\Delta G^{\circ\prime}$ is the driving force for interfacial electron transfer at the solid/liquid contact, λ is the reorganization energy of the reactants in the charge-transfer process, k is the Boltzmann constant, and T is the temperature.

Estimation of κ_{el} is less well documented. A model based on an adaptation of Marcus' theory for liquid/liquid interfaces has recently been used to estimate values of κ_{el} for semiconductor/liquid contacts.[3,7] For reactions at optimal exoergicity, $\kappa_n = 1$ and $k_{et} = k_{et,max}$, so measurement of $k_{et,max}$ would allow experimental evaluation of κ_{el}. Although procedures used to estimate $k_{et,max}$ have yielded reasonable agreement with semiclassical estimates and with other qualitative methods of estimating $k_{et,max}$ for a semiconductor electrode,[3] the use of any approach currently available in the literature to estimate $k_{et,max}$ for such systems has recently been criticized.[5,9] To date, although upper limits on k_{et} have been established experimentally[7,18,19] and are consistent with estimates of k_{et} produced by the available theories,[3,7] there appears to be little direct experimental data on values of k_{et} at well-defined semiconductor/liquid interfaces.[3,4,10,20] We describe such measurements, using n-InP electrodes and a series of outer-sphere redox couples, in this work.

The flux of electrons from the conduction band edge of a semiconductor to a molecular electron acceptor species dissolved in the solution is given by[17]

$$J_{et}(E) = qk_{et}n_s(E)[A] \quad (2)$$

where J_{et} (A cm^{-2}) is the current density due to the direct charge-transfer process, E (V) is the applied potential, q (C) is

* To whom correspondence should be addressed.

[⊗] Abstract published in *Advance ACS Abstracts,* March 1, 1997.

S1089-5647(96)02570-9 CCC: $14.00

the elementary charge, n_s (cm^{-3}) is the electron concentration at the surface of the semiconductor, and [A] (cm^{-3}) is the concentration of acceptors that participate in the electron-transfer process. The surface electron concentration is measured in units of cm^{-3} rather than cm^{-2}, because it is related to the electron concentration in the bulk, n_b, through a Boltzmann relationship:[21]

$$n_s(E) = n_b e^{-q(E+V_{bi})/(kT)} \quad (3)$$

In eq 3, V_{bi} is the built-in voltage developed across the space charge layer in the semiconductor at charge-transfer equilibrium of the semiconductor/liquid contact and n_b is taken to be equal to the dopant density of the semiconductor, N_d.

Thus, the two variables in a semiconductor/liquid system that must be measured in order to evaluate the electron-transfer rate constant using steady-state methods are V_{bi} and $J_{et}(E)$. For a system in which eq 2 is the rate law, J_{et} varies linearly with n_s (i.e., exponentially with E, under forward bias) and varies linearly with [A]. When these criteria are obeyed, eqs 2 and 3 can be used to determine the value of k_{et}, provided that V_{bi} can be determined experimentally. Measurements of k_{et} for solid/liquid contacts having various values of $\Delta G^{\circ\prime}$ can then yield a value for $k_{et,max}$ and, in turn, can allow estimation of κ_{el}.

II. Experimental Section

A. Electrodes and Materials. Nominally undoped ($N_d = 6.4 \times 10^{15}$ cm^{-3}), (100)-oriented, n-type InP wafers were obtained from Crysta-Comm, Inc. and from Sumitomo Electric Industries, Ltd. The samples were sliced into pieces ranging from 0.1 to 0.3 cm^2 in area and were fashioned into electrodes using procedures that have been described previously in the literature.[7] The exposed areas of the electrodes were determined photographically, and the active area was assumed to be equal to the geometric area of the exposed electrode surface. Electrodes were etched by alternately immersing the sample two times each for 30 s into solutions of 0.05% Br_2 (v/v) in CH_3OH and 4.0 M NH_3 in CH_3OH, followed by rinsing with CH_3OH after each immersion.[22] Each electrode was etched immediately before use in electrochemical experiments.

All solvents were dried and distilled under N_2(g) and were then stored under an anaerobic atmosphere. CH_3OH (EM Science) was dried over magnesium methoxide. Tetrahydrofuran (THF, EM Science) was predried over KOH pellets, then transferred to the solvent still, dried over sodium metal (with benzophenone as an indicator), and distilled. The ferrocenes (ferrocene, Fc; 1,1′-dimethylferrocene, Me_2Fc; and decamethylferrocene, $Me_{10}Fc$) were obtained from Strem or Aldrich and were purified by sublimation. The tetrafluoroborate salts of each ferrocene ($FcBF_4$, Me_2FcBF_4, and $Me_{10}FcBF_4$) were prepared using the method of Hendrickson et al.[23] The dichloride salt of 1,1′-diphenyl-4,4′-dipyridinium ($PVCl_2$) was prepared using the synthesis of Kamogawa et al.[24] 1,1′-Diphenyl-4,4′-dipyridinium radical cation ($PV^{+\bullet}$) was produced by electrolysis (vide infra). $LiClO_4$ was dried by fusion at 240 °C in vacuo, and LiCl was dried by heating at 220 °C for at least 6 h in vacuo. All redox couples and electrolytes were stored in a nitrogen-purged drybox until use.

B. Electrochemical Cells and Instrumentation. Electrochemical cells were prepared inside a nitrogen-purged drybox by introducing the solid components of the solution into the cell. The cells were then transferred to a Plexiglas glovebox that contained an anaerobic atmosphere, and the appropriate solvent was introduced. CH_3OH was used as the solvent for all redox systems except $Me_{10}Fc^{+/0}$, for which a solution of 75% CH_3OH−25% THF (v/v) was required to dissolve the redox species at the desired concentrations. $LiClO_4$ was used as the electrolyte in all solutions except in $CH_3OH-PV^{2+/+\bullet}$ cells, where LiCl was required in order to avoid precipitation of the redox species. In all cases, 1.00 M electrolyte was used. All experiments were conducted within the Plexiglas box which contained less than 10 ppm of O_2 as monitored by the lack of any visibly detectable fumes arising from diethylzinc.

In the $CH_3OH-PV^{2+/+\bullet}$ cells, the reduced form of the redox couple was generated electrochemically. A platinum gauze electrode was used as the working electrode and a second platinum gauze electrode, separated from the main solution by a glass frit, was used as the counter electrode. A reference electrode (a methanolic saturated calomel electrode, MSCE) with a potential of −50.0 mV vs SCE was made according to conventional SCE fabrication procedures, except that CH_3OH saturated with LiCl was substituted for the more conventional saturated KCl(aq) solution.[25] The $PV^{+\bullet}$ was generated by applying a potential of −100 to −200 mV vs MSCE across the cell (more negative potentials produced some PV^0). The progress of the electrolysis was monitored both by counting the number of coulombs passed through the cell and by periodically checking the cell potential vs the MSCE reference electrode.

In all electrochemical experiments, after the desired ratio of the oxidized to reduced forms of the redox couple was obtained, the n-InP electrode was etched and immersed into the electrolyte. All electrochemical experiments with semiconducting electrodes were conducted in a three-electrode setup, with a Pt gauze counter electrode and a Pt wire reference. An EG&G Princeton Applied Research (PAR) Model 173 potentiostat in conjunction with an EG&G PAR Model 175 Universal Programmer was used for all current density vs potential measurements. The data were collected on a Houston Instruments Omnigraphic 2000 recorder and in some cases were also fed directly into a computer. Data acquisition and analysis were performed using LabView software (National Instruments, Inc.). Impedance spectra were obtained on a computer-controlled Schlumberger Model 1260 frequency response analyzer equipped with a Model 1286 electrochemical interface. After each set of experiments, the solution potential, $E(A/A^-)$, was measured to ensure that the cell composition had not changed significantly during the course of the experiment.

C. Current Density vs Potential and Built-in Voltage Measurements. For kinetic studies, the current density vs potential ($J-E$) behavior of each electrode was measured in the dark in a cell containing the desired concentration of the redox acceptor species. The $J-E$ data were collected at a scan rate of 50 mV s^{-1}. Each electrode was then re-etched and the series of experiments was repeated, changing the redox acceptor concentration by 10-fold. In some cases, instead of just lowering the acceptor concentration by a factor of 10, the entire solution was diluted with solvent containing 1.00 M electrolyte in order to maintain a constant cell potential. This procedure was necessary for $PV^{2+/+\bullet}$ cells because changing only the acceptor concentration made the cell potential sufficiently negative to form an ohmic contact to the n-InP. Also, in the case of n-InP/$Fc^{+/0}$ contacts, the band edges were found to shift upon increasing the acceptor concentration, so the dilution method was used to examine the concentration dependence of the interfacial kinetics at fixed V_{bi} values. For some experiments, the electrodes were not etched between $J-E$ experiments; in such instances, after running $J-E$ curves in the second solution, the electrodes were returned to the original solution, again without etching, and a third set of $J-E$ data was obtained. The

purpose of these experiments was to determine whether a shift in the $J-E$ behavior was due to the changing acceptor concentration or to some irreversible reaction occurring at the electrode surface. All $J-E$ curves were corrected for the series resistance present in the cell, with the series resistance either determined from impedance measurements (vide infra) or from the $J-E$ behavior of a platinum electrode of similar size and shape to that of the n-InP electrode positioned in the same cell geometry.

The built-in voltage of each n-InP/liquid junction was calculated from the electrochemical impedance data. Data were collected only for cells containing at least 0.010 M of both the oxidized and reduced forms of the redox couple and which contained a counter electrode having at least 10 times the surface area of the working electrode. These precautions were necessary to obtain reliable impedance data.[7] Impedance data were fit to an equivalent circuit consisting of a resistor R_{sc} (representing the resistance to Faradaic charge transfer) in parallel with a capacitor C_{sc} (representing the differential capacitance of the semiconductor space charge region), both in series with a resistance R_s (representing the series resistance due to resistive losses through the cell, leads, etc.). The differential capacitance of the space charge layer is related to the built-in voltage of the junction through the Mott−Schottky equation:[17,21]

$$C_{sc}^{-2} = \frac{2}{q\epsilon\epsilon_0 N_d A_s^2}\left(E + V_{bi} - \frac{kT}{q}\right) \tag{4}$$

where ϵ_0 is the permittivity of free space, ϵ is the dielectric constant, and A_s is the area of the semiconductor electrode. Thus, by measurement of the impedance data at several different potentials, V_{bi} was determined for the semiconductor/liquid interface of interest.

For each dc bias, the impedance, Z, of the cell was measured by superimposing an ac signal of 10 mV rms amplitude on the applied dc potential. The ac frequency was varied from 0.1 to 10^3 kHz, but only data that were almost purely capacitive in nature (phase angle $>80°$) were used in the Mott−Schottky analyses. The differential capacitance, assumed in this equivalent circuit model to be equal to the differential space-charge capacitance of the semiconductor, C_{sc}, was extracted from Z_{im}, the imaginary part of the measured Z, from the equation[26]

$$2\pi f C_{sc} = \frac{1 + (1 - 4(Z_{im}/R_{sc})^2)^{1/2}}{2Z_{im}} \tag{5}$$

In eq 5, f is the frequency of the ac voltage and R_{sc} was taken as the diameter of the semicircle formed by plotting Z_{im} vs Z_{real} for the whole frequency range, where Z_{real} is the real component of the measured impedance.

The equivalent circuit used to model the data was validated by two methods. First, since the Mott−Schottky expression should be independent of the measurement frequency, electrodes which did not show measured capacitances that were independent of frequency (over at least 1 order of magnitude in frequency) were considered defective and were discarded. Second, the slope of the Mott−Schottky plot should be dependent only on the properties of the semiconductor itself (eq 4). The validity of the equivalent circuit model was thus assessed by extracting the dopant density from the slope of the Mott−Schottky plot and comparing it to the value reported by the manufacturer. Only data that showed linear Mott−Schottky plots ($R^2 \geq 0.999$, where R is the correlation coefficient) with calculated dopant densities within 50% of the reported dopant density were considered valid.

III. Results

A. Rate Constant Measurements for n-InP/CH_3OH-$Me_2Fc^{+/0}$ Contacts. Figure 1a shows the $J-E$ behavior of several n-InP/CH_3OH-$Me_2Fc^{+/0}$ contacts in the absence of illumination. In this series of experiments, the concentration of Me_2Fc was held constant at 0.100 M while the concentration of Me_2Fc^+ was either 0.100, 0.010, or 0.001 M. The data were corrected for series resistance and referenced to MSCE for all three concentrations of Me_2Fc^+.

The data of Figure 1a can be fit to the diode equation:[27]

$$J = J_0(e^{-qE/AkT} - 1) \tag{6}$$

where A is the diode quality factor and J_0 is the exchange current density of the semiconductor/liquid contact. In sufficiently far forward bias ($-E \gg AkT/q$), the exponential term dominates the right-hand side of eq 6, and the expression can be rewritten as

$$\ln J = \ln J_0 - \frac{qE}{AkT} \tag{7}$$

Fitting the data of Figure 1a to eq 7 yielded diode quality factors of 1.15, 1.28, and 1.34 for Me_2Fc^+ concentrations of 0.100, 0.010, and 0.001 M, respectively. The deviation from the ideally expected value of $A = 1.0$ for these junctions may arise from a different recombination mechanism contributing to the current density at lower potentials, but the general behavior was in accord with the first-order kinetic dependence of J on the concentration of electrons at the surface of the semiconductor.

For the two higher concentrations of Me_2Fc^+, the separation of the data along the abscissa was 75 ± 5 mV, which is close to the ideally expected 59 mV value derived from eqs 2 and 3.[28] Changing the acceptor concentration by 2 orders of magnitude resulted in a potential difference in the $J-E$ data of 125 ± 5 mV relative to a MSCE reference, compared to the ideal shift of 122 mV that should be produced as a result of changing the Nernst potential of these solutions. These data verify a first-order dependence of J on the concentration of acceptors in the solution; thus the interfacial flux at this solid/liquid contact was dominated by electron transfer from the conduction band to the redox acceptor in the solution phase.

Figure 1b displays the $C_{sc}^{-2}-E$ data for an n-InP/CH_3OH−0.100 M Me_2Fc−0.010 M Me_2Fc^+ contact. In this plot, C_{sc} was extracted from the impedance data obtained at $f = 100$ kHz and $f = 10$ kHz. The $C_{sc}^{-2}-E$ data were linear and essentially independent of frequency over the measurement range. The calculated dopant density was 8.7×10^{15} cm^{-3}, while that reported by the supplier of this wafer was 6.4×10^{15} cm^{-3}. Use of eq 4 yielded a built-in voltage of $V_{bi} = 0.64 \pm 0.01$ V for the solid/liquid contact of Figure 1b.

The impedance analysis was also performed for solutions having a higher concentration of $Me_2Fc^{+/0}$ in order to ensure that the band edge positions of the semiconductor were relatively fixed as the solution acceptor concentration was changed. Figure 1c displays the results of a $C^{-2}-E$ plot for an n-InP/CH_3OH−0.100 M Me_2Fc−0.100 M Me_2Fc^+ contact. These data yielded $V_{bi} = 0.69 \pm 0.01$ V. These Mott−Schottky plots also were in good agreement with the reported dopant density and were independent of frequency over the range of frequencies probed in this work. Since the Nernstian potential of the cell, $E(A/A^-)$, in Figure 1c was more positive than that of Figure 1b by 60 mV, the built-in voltage of the contact of Figure 1c was expected to be 60 mV greater than that of Figure 1b. The actual difference was just slightly less than this ideal separation but was in the correct direction, so that a positive shift in

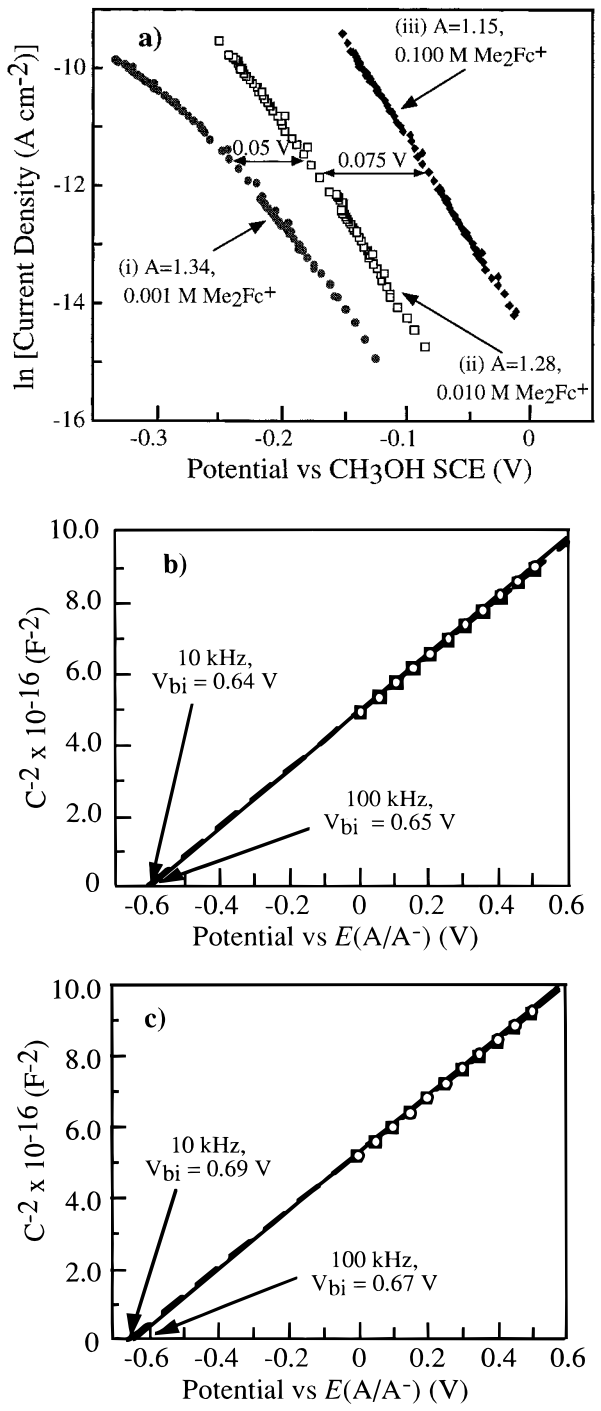

Figure 1. Current density−potential and differential capacitance−potential data for n-type InP/CH_3OH−$Me_2Fc^{+/0}$ contacts. (a) ln J vs E for n-InP/CH_3OH−1.00 M $LiClO_4$−0.100 M Me_2Fc interfaces having Me_2Fc^+ (electron acceptor) concentrations of (i) 0.001 M (E(A/A$^-$) = 0.130 V vs MSCE), (ii) 0.010 M (E(A/A$^-$) = 0.192 V vs MSCE), and (iii) 0.100 M (E(A/A$^-$) = 0.252 V vs MSCE). The diode quality factor, A, was extracted from linear fits of these data to eq 7. (b) Mott−Schottky plots taken at two ac measuring frequencies, 10 kHz (dashed line, solid squares) and 100 kHz (solid line, open circles), for an n-InP/CH_3OH−1.00 M $LiClO_4$−0.100 M Me_2Fc−0.010 M Me_2Fc^+ contact. The potentials are referenced to the Nernstian potential of the cell, E(A/A$^-$). The average dopant density extracted from the slopes of these lines was 8.7×10^{15} cm^{-3}, compared to the reported dopant density of 6.4×10^{15} cm^{-3}. The built-in voltages, V_{bi}, are listed for each frequency. (c) Mott−Schottky plots for two ac measuring frequencies, 10 kHz (dashed line, solid squares) and 100 kHz (solid line, open circles), for an n-InP/CH_3OH−1.00 M $LiClO_4$−0.100 M Me_2Fc−0.100 M Me_2Fc^+ contact. The average dopant density extracted from the slopes of these lines was 8.7×10^{15} cm^{-3}.

E(A/A$^-$) led to an increase in the built-in voltage of the semiconductor/liquid contact.

The energetic information from the $C^{-2}-E$ analysis of Figure 1b,c was then combined with the kinetic information from the $J-E$ data of Figure 1a to evaluate the value of k_{et} for this system. To perform this computation, the built-in voltage obtained from the Mott−Schottky plots was used in eq 3 to compute the surface electron concentration at a given potential in forward bias. Using eq 2, a rate constant value was then computed from the current density observed at the chosen potential. The potentials chosen for evaluation of k_{et} were all ones for which the $J-E$ data were linearly dependent on the acceptor concentration.

For the n-InP−CH_3OH−0.100 M Me_2Fc−0.100 M Me_2Fc^+ interface of Figure 1, this procedure yielded $k_{et} = 6.2 \times 10^{-17}$ cm^4 s^{-1} at $E = -0.45$ V vs E(A/A$^-$). Since the diode quality factors for these junctions were not exactly unity, the calculated values of k_{et} depended slightly on the potential chosen for the kinetic measurements. For instance, a value of $k_{et} = 1.7 \times 10^{-16}$ cm^4 s^{-1} was obtained for the same electrode at a potential of −0.25 V vs E(A/A$^-$). Since kinetic processes with diode quality factors of 1.0 tend to dominate the interfacial flux further into forward bias, the charge-transfer rate constants calculated at the more negative potentials are more likely to reflect the true rate constant.[29]

For the n-InP/CH_3OH−0.100 M Me_2Fc−0.010 M Me_2Fc^+ contact, the computed electron-transfer rate constant varied from 2.2×10^{-17} to 1.2×10^{-16} cm^4 s^{-1} over a potential range of $E = -0.45$ to −0.25 V vs E(A/A$^-$). Thus, these k_{et} values were consistent with those derived for the higher Me_2Fc^+ acceptor concentration, confirming the bimolecular nature of the observed interfacial kinetic process.

At any individual potential, repeated determinations of $J-E$ and $C_{sc}^{-2}-E$ were performed, and the resulting values for k_{et} were analyzed using conventional statistical procedures. Results from many different electrodes yielded an average charge-transfer rate constant of $(8.5 \pm 7.7) \times 10^{-17}$ cm^4 s^{-1} for n-InP/CH_3OH−0.100 M Me_2Fc−0.100 M Me_2Fc^+ contacts and yielded $k_{et} = 1.1 \times 10^{-16}$ cm^4 s^{-1} for InP/CH_3OH−0.100 M Me_2Fc−0.0100 M Me_2Fc^+ contacts. The standard deviation of k_{et} for InP/CH_3OH−0.100 M Me_2Fc−0.0100 M Me_2Fc^+ contacts slightly exceeded the mean value of k_{et} for this system, with individual k_{et} values ranging from 1.5×10^{-18} to 9.9×10^{-16} cm^4 s^{-1}. The second highest (of 24 values) calculated rate constant was 3.6×10^{-16} cm^4 s^{-1}. Given the error present in the measurements, k_{et} for the n-InP/CH_3OH-$Me_2Fc^{+/0}$ junction was estimated to be $(1-10) \times 10^{-17}$ cm^4 s^{-1}.

B. Rate Constant Measurements for n-InP/CH_3OH-(75%)−THF(25%)−$Me_{10}Fc^{+/0}$ Contacts. Analogous experiments were performed for n-InP/$Me_{10}Fc^{+/0}$ contacts. In this system, due to the low solubility of $Me_{10}Fc$ in pure CH_3OH, the solvent was 75% CH_3OH/25% THF (v/v). $J-E$ data were collected for [$Me_{10}Fc$] = 0.025 M with the acceptor concentration adjusted to produce [$Me_{10}Fc^+$] = 0.025 M or [$Me_{10}Fc^+$] = 0.0025 M (Figure 2a). Although the diode quality factors of these contacts deviated somewhat from unity, the data for the two $Me_{10}Fc^+$ concentrations were separated by the expected ≈60 mV relative to MSCE. Thus, the reaction was kinetically first order in the concentration of solution acceptors and in the electron concentration at the semiconductor surface, as predicted by the rate law of eq 2.

Figure 2b displays the Mott−Schottky plots for n-InP/CH_3OH−THF−0.025 M Me_2Fc−0.025 M $Me_{10}Fc^+$ contacts at $f = 39.811$ kHz and $f = 3.981$ kHz. For these contacts, the range over which the impedance data were independent of

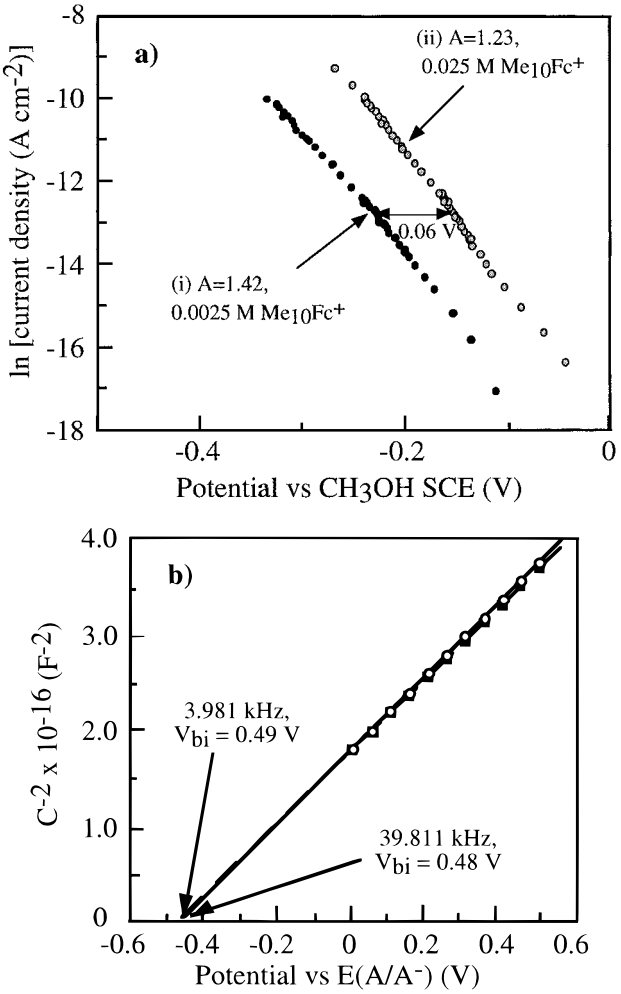

Figure 2. Data for n-InP/$CH_3OH-THF-Me_{10}Fc^{+/0}$ contacts. (a) ln J vs E data for n-InP/$CH_3OH-THF-1.00$ M $LiClO_4-0.025$ M $Me_{10}Fc$ contacts having $Me_{10}Fc^+$ concentrations of (i) 0.0025 M ($E(A/A^-) = -0.042$ V vs MSCE) and (ii) 0.025 M ($E(A/A^-) = 0.010$ V vs MSCE). The diode quality factor, A, was extracted from linear fits of these data to eq 7. (b) Mott−Schottky plots for two ac measuring frequencies, 3.981 kHz (dashed line, solid squares) and 39.811 kHz (solid line, open circles), for an n-InP/$CH_3OH-THF-1.00$ M $LiClO_4-0.025$ M $Me_{10}Fc-0.025$ M $Me_{10}Fc^+$ contact. The average dopant density extracted from the slopes of these lines was 9.5×10^{15} cm^{-3}. The built-in voltages, V_{bi}, are listed for each frequency.

frequency was somewhat smaller than that observed for *n*-InP/$CH_3OH-Me_2Fc^{+/0}$ contacts, but the impedance data were nevertheless essentially independent of frequency over an order of magnitude of f. Over this frequency range, the dopant density computed from the $C^{-2}-E$ data was in good agreement with the known dopant density of the sample. The built-in voltage obtained from the $C^{-2}-E$ analysis of this sample was 0.49 ± 0.01 V.[30]

The same procedure as described in section III.A, in which the analyses of $C^{-2}-E$ and $J-E$ data were combined, was used to compute the value of k_{et} for the n-InP/$CH_3OH-THF-Me_{10}Fc^{+/0}$ contacts. For the data shown in Figure 2, $k_{et} = 1.2 \times 10^{-17}$ cm^4 s^{-1} at $E = -0.35$ V vs $E(A/A^-)$ and $k_{et} = 4.9 \times 10^{-17}$ cm^4 s^{-1} at $E = -0.15$ V vs $E(A/A^-)$. Over several trials, the average electron-transfer rate constant for this system was found to be 5.3×10^{-17} cm^4 s^{-1}, but individual values ranged from 9.3×10^{-18} to 6.6×10^{-17} cm^4 s^{-1}. Within the experimental error afforded by the relatively small uncertainties in V_{bi} (propagating into larger uncertainties in n_s), along with differences in k_{et} determined at different measurement potentials (due to the deviation of A from the ideal value of $A = 1.0$), these k_{et} values were indistinguishable from those reported above for n-InP/$CH_3OH-Me_2Fc^{+/0}$ contacts.

C. Rate Constant Data for n-InP/$CH_3OH-PV^{2+/+\bullet}$ Contacts. Cyclic voltammetric data showed that $PV^{2+/+\bullet}$ exhibited reversible, one-electron redox behavior in CH_3OH at a Pt electrode. This redox couple displayed a formal potential, $E^{\circ\prime}(A/A^-)$, of −180 mV vs MSCE, which was >200 mV more negative than $E^{\circ\prime}(A/A^-)$ for $Me_{10}Fc^{+/0}$ (in $CH_3OH-THF$). Consequently, the more negative value of $E^{\circ\prime}(A/A^-)$ for $PV^{2+/+\bullet}$ should produce smaller built-in voltages, and therefore lower values of $\Delta G^{\circ\prime}$, for n-InP/$CH_3OH-PV^{2+/+\bullet}$ contacts relative to those of n-InP/CH_3OH-$Me_2Fc^{+/0}$ or n-InP/$CH_3OH-THF-Me_{10}Fc^{+/0}$ junctions.

Figure 3a shows the $J-E$ data for an n-InP electrode in contact with $CH_3OH-1.00$ M $LiCl-0.050$ M $PV^{2+}-0.010$ M $PV^{+\bullet}$. In this system, J_0 was sufficiently large that the condition $-E > AkT/q$ was not satisfied where the current density was accurately measurable without large overpotential corrections. Thus, the simplifications that allow eq 6 to be transformed into eq 7 were not appropriate for this system. The kinetic data of Figure 3a were therefore fit to eq 6 to yield J_0, and then k_{et} was computed using eq 2, with $n_s(E) = n_s(0)$.

Since the redox potential of the solution was near the InP conduction band edge energy at the semiconductor surface, the $J-E$ behavior for this n-InP/liquid contact was very sensitive to the value of $E(A/A^-)$. For example, at even slightly more negative potentials than $E(A/A^-) = -0.150$ mV vs MSCE, the n-InP/liquid contact exhibited nonrectifying, near-ohmic behavior. It was therefore not possible to perform an experiment analogous to that described in Figure 1 with the n-InP/$PV^{2+/+\bullet}$ contacts, in which the acceptor concentration was decreased in order to reveal the kinetic dependence of J on [A] while [A^-] was held constant. Instead, the $J-E$ properties of an n-InP electrode were recorded in contact with a $CH_3OH-1.00$ M $LiCl-0.010$ M $PV^{2+}-0.050$ M $PV^{+\bullet}$ solution and then in contact with a $CH_3OH-1.00$ M $LiCl-0.0010$ M $PV^{2+}-0.0050$ M $PV^{+\bullet}$ solution. The latter solution was prepared by diluting part of the more concentrated solution with 1.00 M LiCl in CH_3OH. This procedure allowed investigation of the desired kinetic behavior but required a slightly different analysis of the data, as described below.

The results of this experiment are shown in Figure 3b. In this figure, the current scale for the electrode in the more dilute solution is multiplied by a factor of 10. These data clearly show the first-order dependence of the current density on the concentration of acceptor species dissolved in the solution, as expected from eq 2.

The Mott−Schottky plots for two ac frequencies applied to the $CH_3OH-1.00$ M $LiCl-0.010$ M $PV^{2+}-0.050$ M $PV^{+\bullet}$ interface are shown in Figure 3c. The impedance data for this junction exhibited more frequency dispersion than is evident in Figures 1c or 2b, possibly due to the large Faradaic current that was present during the impedance measurements of this low barrier height system. Despite this complication, the dopant density obtained from the $C^{-2}-E$ plots over the frequency range 158.489−15.849 kHz was within 30% of the value specified by the manufacturer. Additionally, although the slopes varied slightly over this range of frequencies, the x intercepts of the $C^{-2}-E$ plots were in agreement to within ±15 mV. The built-in voltage of this junction was calculated to be 0.28 V, yielding an electron-transfer rate constant of 3.3×10^{-16} cm^4 s^{-1}. Over many measurements of this system, the average electron-transfer rate constant was $k_{et} = (3.3 \pm 2.4) \times 10^{-16}$ cm^4 s^{-1}. In this case, the range of values for the electron-transfer rate constant was higher than those reported for the n-InP/CH_3OH-$Me_2Fc^{+/0}$

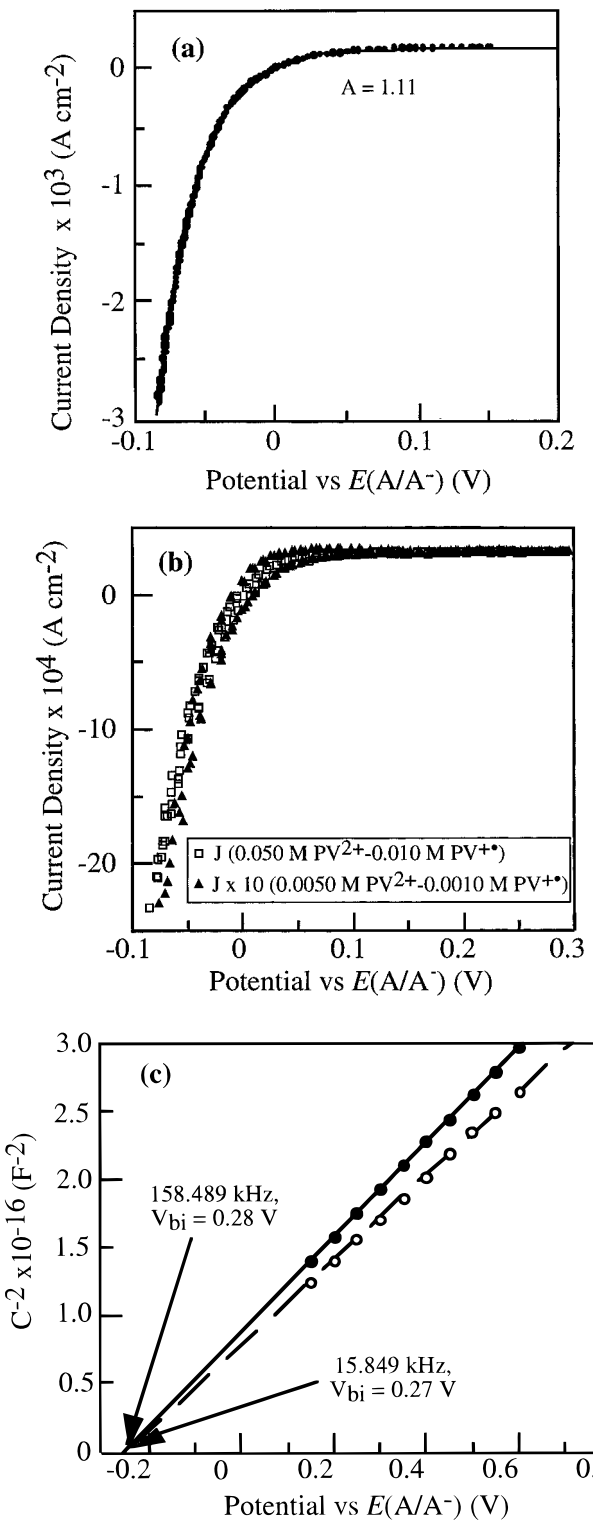

Figure 3. Data for n-InP/CH_3OH−1.00 M LiCl−$PV^{2+/+\bullet}$ contacts. (a) $J-E$ data for an n-InP/CH_3OH−1.00 M LiCl−0.050 M PV^{2+}−0.010 M $PV^{+\bullet}$ contact (E(A/A$^-$) = −0.146 V vs MSCE). The data were fit to eq 6 and yielded a diode quality factor of 1.1. (b) $J-E$ data for n-InP/CH_3OH−1.00 M LiCl−0.050 M PV^{2+}−0.010 M $PV^{+\bullet}$ and n-InP/CH_3OH−1.00 M LiCl−0.0050 M PV^{2+}−0.0010 M $PV^{+\bullet}$ contacts. The current density data for the n-InP/CH_3OH−1.00 M LiCl−0.0050 M PV^{2+}−0.0010 M $PV^{+\bullet}$ contact (triangles) has been multiplied by 10 for better comparison to the data for the CH_3OH−1.00 M LiCl−0.050 M PV^{2+}−0.010 M $PV^{+\bullet}$ solution (open squares). (c) Mott−Schottky plots for the system in (a) at two ac measuring frequencies, 15.849 kHz (dashed line, open circles) and 158.489 kHz (solid line, filled circles). The dopant density predicted from the slope of the 15.849 kHz line was 9.9×10^{15} cm^{-3}, while the dopant density extracted from the slope of the 158.489 kHz line was 8.9×10^{15} cm^{-3}. The built-in voltages, V_{bi}, are listed for each frequency.

and n-InP/CH_3OH−THF−$Me_{10}Fc^{+/0}$ interfaces, with k_{et} ranging from 1×10^{-16} to 9×10^{-16} cm^4 s^{-1}. It should be noted, however, that the reorganization energies for the viologens in homogeneous solution are significantly lower than those of the ferrocenes;[31−33] hence the decreased outer-sphere reorganization energies of this redox system somewhat counteracted the effects of the lower driving force at the n-InP/$PV^{2+/+\bullet}$ contact.

D. n-InP/CH_3OH−$Fc^{+/0}$ Contacts. Figure 4a depicts the $J-E$ characteristics of n-InP/CH_3OH−0.010 M Fc−0.100 M Fc^+ and n-InP/CH_3OH−0.010 M Fc−0.010 M Fc^+ contacts. In contrast to the behavior of the n-InP/CH_3OH interfaces described above, the n-InP/CH_3OH−$Fc^{+/0}$ junction showed a shift in its $J-E$ properties of 120 mV vs MSCE upon increasing the acceptor concentration by an order of magnitude. This shift was approximately twice as large as the ≈60 mV shift that was observed for the other redox systems (Figures 1 and 2), and is twice as large as that expected from the rate law of eq 2. This $J-E$ behavior indicated a shift in the band edge positions of the semiconductor as the Nernstian potential of the $Fc^{+/0}$ solution increased, and precluded a straightforward justification of the second-order rate law by variation of [A] with constant [A$^-$]. This band edge movement may arise from a number of sources, including surface state charging or carrier inversion and does not necessarily indicate any adsorption of the Fc^+ ion on the electrode surface.

To minimize such band-edge shifts, the concentrations of Fc^+ and Fc were changed simultaneously but the [A]/[A$^-$] ratio was held fixed, so that the Nernstian potential of the solution was held constant. To implement this process, part of a CH_3OH−1.00 M $LiClO_4$−0.010 M Fc−0.100 M Fc^+ solution was diluted with sufficient CH_3OH−1.00 M $LiClO_4$ to form a CH_3OH−1.00 M $LiClO_4$−0.0010 M Fc−0.010 M Fc^+ solution. This method is identical with the one used to prove second-order kinetics for the n-InP/CH_3OH−$PV^{2+/+\bullet}$ system (vide supra). Figure 4b shows the $J-E$ behavior for an n-InP electrode in contact with each solution and illustrates the 70 mV potential shift of the $J-E$ behavior, relative to a fixed reference, that was observed when this experimental protocol was used.

Impedance data were again used to obtain the energetics for the n-InP/CH_3OH−$Fc^{+/0}$ interface. Figure 4c,d display the impedance data for representative n-InP/CH_3OH−0.010 M Fc−0.100 M Fc^+ and n-InP/CH_3OH−0.010 M Fc−0.010 M Fc^+ contacts, respectively, in the form of Mott−Schottky plots. These $C^{-2}-E$ plots showed little frequency dispersion and had slopes that were consistent with those computed from the dopant density reported by the manufacturer of the InP samples. In addition, the built-in voltages of these two n-InP/CH_3OH−$Fc^{+/0}$ contacts were essentially indistinguishable from each other. This effect was observed for several different electrodes; in fact, the mean value of V_{bi} for the n-InP/CH_3OH−0.010 M Fc−0.100 M Fc^+ contact, $V_{bi} = 0.78$ V, was slightly lower than the mean value of $V_{bi} = 0.81$ V measured for the n-InP/CH_3OH−0.010 M Fc−0.010 M Fc^+ contact. The 120 mV shift observed in the $J-E$ data when [Fc^+] was varied but [Fc] was held constant is thus readily understood in the context of the band edge movement revealed by the $C^{-2}-E$ data. As displayed in Figure 4c,d, the built-in voltage of the more concentrated Fc^+ solution is lower than expected by ≈60 mV, due to a band edge shift that is consistent with prior studies of n-InP/nonaqueous liquid contacts having such positive Nernstian solution potentials.[13] This band edge movement results in an additional 60 mV shift in the $J-E$ curves for these solutions relative to that expected from the rate law of eq 2 assuming fixed band edge positions, thus resulting in the 120 mV shift in $J-E$ behavior (vs the MSCE reference) observed in Figure 4a.

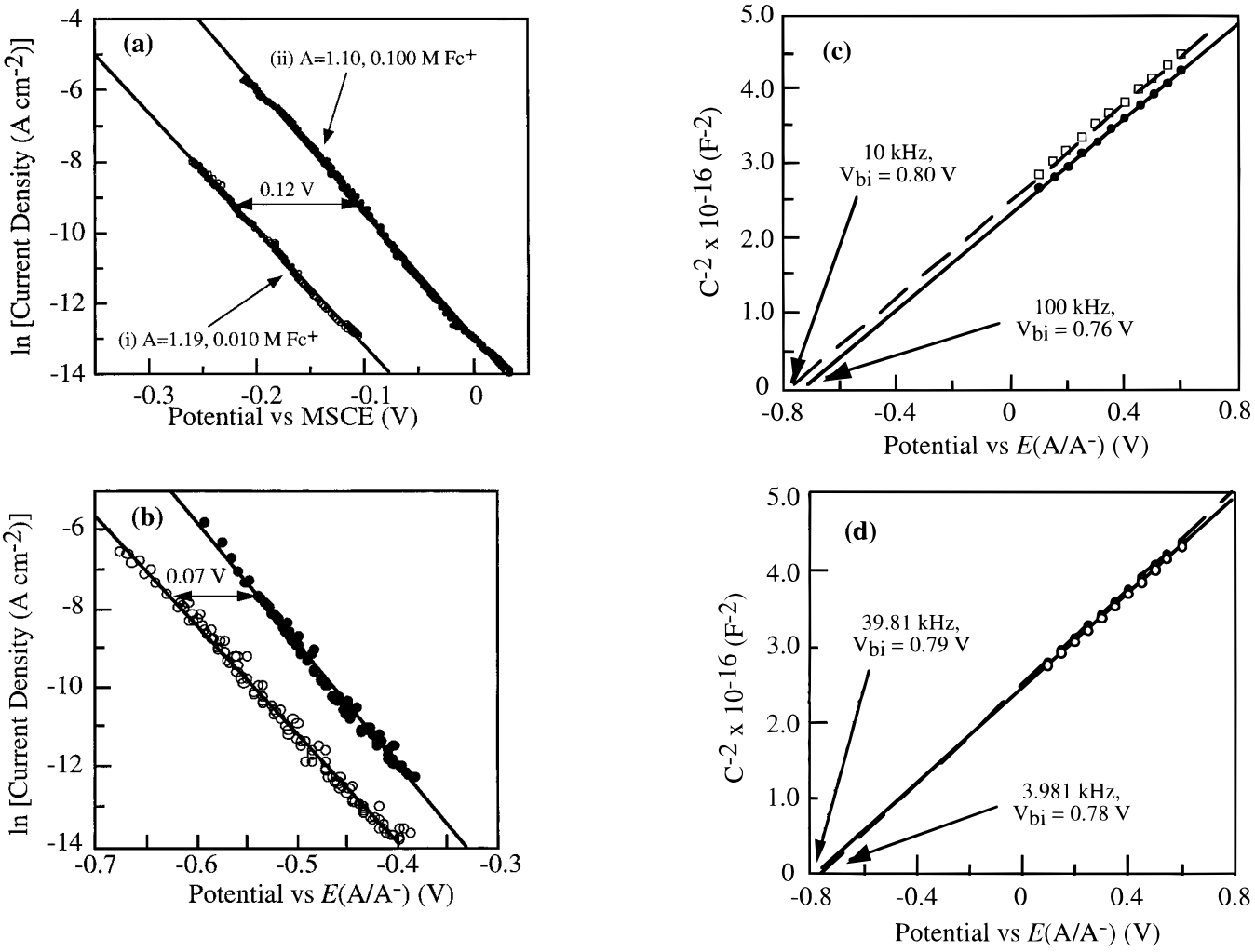

Figure 4. Data for n-InP/$CH_3OH-Fc^{+/0}$ contacts. (a) $J-E$ data for n-InP/$CH_3OH-1.00$ M $LiClO_4-0.010$ M Fc contacts having Fc^+ concentrations of (i) 0.010 M ($E(A/A^-) = 0.350$ V vs MSCE), and (ii) 0.100 M ($E(A/A^-) = 0.407$ V vs MSCE). (b) ln J vs E data for an n-InP/$CH_3OH-1.00$ M $LiClO_4-0.010$ M $Fc-0.100$ M Fc^+ ($E(A/A^-) = 0.406$ V vs MSCE) contact (filled circles) and for an n-InP/$CH_3OH-1.00$ M $LiClO_4-0.0010$ M $Fc-0.010$ M Fc^+ ($E(A/A^-) = 0.403$ V vs MSCE) contact (open circles). (c) Mott−Schottky plots for two ac measuring frequencies, 10 kHz (dashed line, open squares) and 100 kHz (solid line, filled circles), for an n-InP/$CH_3OH-1.00$ M $LiClO_4-0.010$ M $Fc-0.010$ M Fc^+ interface. The average dopant density extracted from the slopes of these lines was 8.1×10^{15} cm^{-3}. The built-in voltages, V_{bi}, are listed for each frequency. (d) Mott−Schottky plots for two ac measuring frequencies, 3.981 kHz (dashed line, filled circles) and 39.811 kHz (solid line, open circles), for an n-InP/$CH_3OH-1.00$ M $LiClO_4-0.010$ M $Fc-0.100$ M Fc^+ contact. The average dopant density extracted from the slopes of these lines was 8.2×10^{15} cm^{-3}.

With the energetics available from the impedance analysis, k_{et} could be computed for each n-InP/$CH_3OH-Fc^{+/0}$ solution from the combined analysis of $C^{-2}-E$ and $J-E$ data. For the n-InP/$CH_3OH-0.010$ M $Fc-0.100$ M Fc^+ contact, the average electron-transfer rate constant was found to be $(5.3 \pm 3.2) \times 10^{-17}$ cm^4 s^{-1}, while for the n-InP/$CH_3OH-0.010$ M $Fc-0.010$ M Fc^+ contact, the average k_{et} value was $(1.6 \pm 1.1) \times 10^{-16}$ cm^4 s^{-1}. Table 1 summarizes the kinetic data obtained for all of the InP/liquid contacts studied in this work.

TABLE 1: Summary of Electron-Transfer Rate Constants[a]

redox couple	[A] (M)	k_{et} (cm^4 s^{-1})
$Me_2Fc^{+/0}$	0.100	8.5×10^{-17}
$Me_2Fc^{+/0}$	0.010	1.1×10^{-16}
$Me_{10}Fc^{+/0}$	0.025	5.3×10^{-17}
$PV^{2+/+\bullet}$	0.050	3.3×10^{-16}
$Fc^{+/0}$	0.100	5.3×10^{-17}
$Fc^{+/0}$	0.010	1.6×10^{-16}

[a] Values listed for k_{et} are statistical averages of many trials for each redox couple at each electron acceptor concentration. The statistical and systematic errors associated with each mean k_{et} value are described in detail in the text.

IV. Discussion

The most significant feature of the n-InP/liquid contacts discussed herein is that they exhibited not only nearly ideal energetic but also nearly ideal kinetic behavior. Ideal energetic behavior, in which the $C^{-2}-E$ plots are well-behaved and the resulting band edge positions are invariant for a wide range of redox potentials, has been observed previously for some n-InP/CH_3CN contacts.[13] The above data document this behavior in detail for a series of outer-sphere redox couples and extend these observations to CH_3OH as the solvent. In addition, the n-InP contacts studied in this work exhibited nearly ideal kinetic behavior in that their current density−potential relationships were observed to obey the rate law behavior expected from eq 2 for a simple interfacial electron-transfer event acting as the dominant recombination process to produce current flow through the semiconductor/liquid interface. Except for recent work on n-Si/liquid contacts in our laboratory,[8] such behavior has not, to our knowledge, been reported previously for a series of outer-sphere, one-electron redox couples at a semiconductor surface, yet this combination of behaviors is required in order to

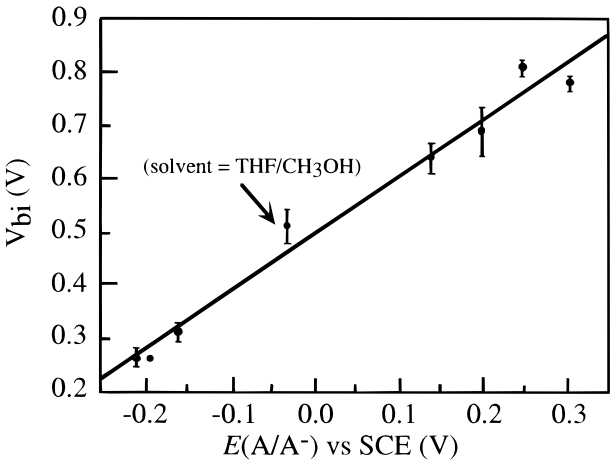

Figure 5. Dependence of the built-in voltage of n-InP electrodes on the Nernstian potential, $E(A/A^-)$, of various contacts having outer-sphere redox systems dissolved in the solution phase. The Nernstian potentials are referenced to SCE and differ from the values measured experimentally against a methanolic SCE by 50.0 mV. The equation for the best-fit line (omitting the point for $Me_{10}Fc^{+/0}$, which was obtained in a different solvent system) yields a slope of 1.09. Extrapolating the graph to $V_{bi} = 0$ V and correcting for the difference between the potential of the conduction band edge, E_{cb}, and the Fermi level of the semiconductor yields $E_{cb} = -0.52$ V vs SCE. However, since the slope is not exactly 1.0, at higher built-in voltages the apparent conduction band edge position is slightly different; for example, taking the specific point determined for n-InP/CH_3OH−1.00 M $LiClO_4$−0.100 M Me_2Fc−0.100 M Me_2Fc^+ of $V_{bi} = 0.69$ V at $E(A/A^-) = 0.19$ V vs SCE, $E_{cb} = -0.62$ V vs SCE.

determine directly the values of the heterogeneous charge-transfer rate constants for semiconductor electrodes from steady-state $J-E$ data.

The ideal energetic behavior reported herein is significant in view of prior hypotheses that n-type InP surfaces exhibit Fermi level pinning in contact with nonaqueous electrolytes.[11,34] In the absence of Fermi level pinning, the difference in the built-in voltage of two semiconductor/liquid junctions should be equal to the difference in the Nernstian potentials of the two electrolyte solutions. Figure 5 shows the built-in voltage as a function of $E(A/A^-)$ for the junctions examined in this work. The points define a straight line, with the exception of those for the CH_3OH−1.00 M $LiClO_4$−0.010 M Fc−0.100 M Fc^+ solution, where the junction is no longer sensitive to the cell potential, and the $Me_{10}Fc^{+/0}$ solution, where a different solvent system was used because of solubility constraints. Fitting the remaining points to a line yielded a slope of 1.1, indicating that these junctions behave nearly ideally over this potential range. Thus, for this series of contacts, the equilibrium band bending and equilibrium electric field strength in the n-InP are not dominated by surface states but instead respond completely to variation of the thermodynamic properties of the redox species in the liquid phase. This conclusion is in agreement with the photovoltage behavior of n-InP/CH_3CN contacts[12] but contrasts with earlier, nonideal $C^{-2}-E$ data that were interpreted within a complex equivalent circuit model to indicate nearly complete Fermi level pinning for n-type InP electrodes in contact with CH_3CN solvent.[34] It also contrasts with the well-documented Fermi level pinning behavior of metal−semiconductor Schottky contacts formed on n-type InP surfaces.[35,36]

The kinetic behavior of these n-InP/CH_3OH contacts is also significant in the context of theoretical expectations for heterogeneous charge-transfer rate constants at semiconductor/liquid interfaces. Since the $\Delta G^{\circ\prime}$ values for the reported contacts were between −0.4 and −0.9 eV and the reorganization energies of the redox couples used in this work were ≈0.5−1.0 eV,[31−33] the value of k_{et} is expected to be dominated by the electronic terms of the rate constant expression, as opposed to the nuclear (Franck−Condon) factors. For example, for the $Me_{10}Fc^{+/0}$ redox couple, the reorganization energy is predicted to be about 0.80 eV,[33] while n-InP in contact with this redox system yielded $\Delta G^{\circ\prime} = -0.6$ eV. Substituting these numbers into eq 1 yields $\kappa_n = 0.52$, indicating k_{et} for this system is only expected to be about a factor of 2 lower than $k_{et,max}$. Performing a similar calculation for the n-InP/CH_3OH−$PV^{2+/+\bullet}$ system using $\lambda = 0.5$ eV[32,33] and $\Delta G^{\circ\prime} = 0.4$ eV yields $\kappa_n = 0.82$. The value of k_{el} has been previously estimated to be 10^{-30} cm^4 for a typical semiconductor,[3,7] which yields a value of $k_{et,max} = 10^{-17}$ cm^4 s^{-1} at optimal exoergicity, assuming that $\nu_n = 10^{13}$ s^{-1}. The expectations for $k_{et,max}$ and κ_{el} are thus in excellent agreement with the kinetic behavior observed for the n-InP/liquid contacts investigated in this work.

Considering the theoretical prediction in more detail, the value of κ_{el} has been related to the Bohr radius of the electron in the solid. In this approach, the Bohr radius was taken as a qualitative measure of the delocalization length of the wave function for the electron in the conduction band of the semiconductor. Due to the very low effective mass of electrons in the conduction band of n-InP,[21] the Bohr radius of electrons in InP is a factor of 10 larger than that of electrons in Si (or than that of carriers in most other common semiconductors),[37] so the existing model implies that the k_{et} values for n-InP/liquid contacts should be larger, by about an order of magnitude, than those for otherwise identical contacts using other types of semiconductor electrodes. This prediction seems to be borne out experimentally from the available data, because recent steady-state kinetic data obtained on n-type Si/CH_3OH interfaces has yielded $k_{et,max}$ values of ≈5×10^{-17} cm^4 s^{-1} for a series of viologen acceptors.[8] Due to the significant error of these types of $J-E$ and $C^{-2}-E$ kinetic measurements at present, which limits the precision of the determination of $k_{et,max}$ for n-InP/liquid contacts to factors of 5−10, further work would be required to evaluate definitively any experimental relationship between the Bohr radius of the carrier in the solid and the charge-transfer rate constant at the semiconductor/liquid contact. Nevertheless, the data available to date seem to be in qualitative agreement with this prediction of the model for interfacial charge transfer at semiconductor/liquid junctions.[3]

In summary, a combination of energetic and kinetic measurements has been used to determine values of the interfacial charge-transfer rate constants for a series of n-InP/liquid contacts. In all cases, the $J-E$ behavior was in accord with the ideally expected rate law for interfacial charge transfer, being first order in the concentration of acceptors in the solution and approximately first order in the concentration of electrons at the surface of the semiconductor. Mott−Schottky plots derived from impedance measurements were essentially independent of frequency, yielded the theoretically expected slopes, and produced reliable measurements of the built-in voltages and band edge positions of the solid/liquid contacts. The built-in voltages of n-InP/CH_3OH interfaces were found to be controlled by the Nernstian potential of the solution, indicating a lack of Fermi level pinning over most of the potential range investigated. Electron-transfer rate constants for these semiconductor/liquid junctions were determined to be on the order of $10^{-17}-10^{-16}$ cm^4 s^{-1}. These values are in excellent agreement with theoretical models available in the literature for such charge-transfer processes. Taken together with upper limits on $k_{et,max}$ that have been established recently for a wide range of semiconductor/liquid junctions, these data therefore strongly support the theoretical prediction that optimally exoergic steady-state

interfacial charge-transfer rate constants are in the range 10^{-17}–10^{-16} cm^4 s^{-1} for semiconductor surfaces in contact with randomly dissolved, nonadsorbing, outer-sphere redox couples.[3,8]

Acknowledgment. We acknowledge the Department of Energy, Office of Basic Energy Sciences, Fundamental Interactions Branch, for their generous support of this work. K.E.P. also acknowledges the National Science Foundation for a predoctoral fellowship.

References and Notes

(1) Marcus, R. A. *J. Phys. Chem.* **1990**, *94*, 1050.
(2) Gerischer, H. *J. Phys. Chem.* **1991**, *95*, 1356.
(3) Lewis, N. S. In *Annu. Rev. Phys. Chem.* **1991**, *42*, 543.
(4) Koval, C. A.; Howard, J. N. *Chem. Rev. (Washington, D.C.)* **1992**, *92*, 411.
(5) Rosenwaks, Y.; Thacker, B. R.; Nozik, A. J.; Ellingson, R. J.; Burr, K. C.; Tang, C. L. *J. Phys. Chem.* **1994**, *98*, 2739.
(6) Bard, A. J.; Mirkin, M. V.; Horrocks, B. R. *J. Phys. Chem.* **1994**, *98*, 2739.
(7) Pomykal, K. E.; Fajardo, A. M.; Lewis, N. S. *J. Phys. Chem.* **1996**, *100*, 3652.
(8) Fajardo, A. M.; Lewis, N. S. *Science* **1996**, *274*, 5289.
(9) (a) Smith, B. B.; Nozik, A. J. *Chem. Phys.* **1996**, *205*, 47. (b) Smith, B, B.; Halley, J. W.; Nozik, A. J. *Chem. Phys.* **1996**, *205*, 245.
(10) Uhlendorf, I.; Reineke-Koch, R.; Memming, R. *J. Phys. Chem.* **1996**, *100*, 4930.
(11) Dominey, R. N.; Lewis, N. S.; Wrighton, M. S. *J. Am. Chem. Soc.* **1981**, *103*, 1261.
(12) Heben, M. J.; Kumar, A.; Zheng, C.; Lewis, N. S. *Nature* **1989**, *340*, 621.
(13) Koval, C.; Austermann, R. *J. Electrochem. Soc.* **1985**, *132*, 2656.
(14) Marcus, R. A.; Sutin, N. *Biochim. Biophys. Acta* **1985**, *811*, 265.
(15) Marcus, R. A. *J. Chem. Phys.* **1965**, *43*, 679.
(16) Gerischer, H. In *Physical Chemistry: An Advanced Treatise*; Eyring, H., Henderson, D., Yost, W., Eds.; Academic: New York, 1970; Vol. 9A, p 463.
(17) Morrison, S. R. *Electrochemistry at Semiconductor and Oxidized Metal Electrodes*; Plenum: New York, 1980.
(18) Forbes, M. D. E.; Lewis, N. S. *J. Am. Chem. Soc.* **1990**, *112*, 3682.
(19) Howard, J. N.; Koval, C. A. *Anal. Chem.* **1994**, *66*, 4525.
(20) Horrocks, B. R.; Mirkin, M. V.; Bard, A. J. *J. Phys. Chem.* **1994**, *98*, 9106.
(21) Sze, S. M. *The Physics of Semiconductor Devices;* 2nd ed.; Wiley: New York, 1981.
(22) Aspnes, D. E.; Studna, A. A. *Appl. Phys. Lett.* **1981**, *39*, 316.
(23) Hendrickson, D. H.; Sohn, Y. S.; Gray, H. B. *Inorg. Chem.* **1971**, *10*, 1559.
(24) Kamogawa, H.; Sato, S. *Bull. Chem. Soc. Jpn.* **1991**, *64*, 321.
(25) Pomykal, K. E.; Fajardo, A. M.; Lewis, N. S. *J. Phys. Chem.* **1996**, *100*, 3652.
(26) Bard, A. J.; Faulkner, L. R. *Electrochemical Methods: Fundamentals and Applications*; John Wiley & Sons: New York, 1980; p 629.
(27) Tan, M. X.; Laibinis, P. E.; Nguyen, S. T.; Kesselman, J. M.; Stanton, C. E.; Lewis, N. S. *Prog. Inorg. Chem.* **1994**, *41*, 21.
(28) Rosenbluth, M. L.; Lewis, N. S. *J. Phys. Chem.* **1989**, *93*, 3735.
(29) The observed current at the semiconductor interface is given by the sum of the currents for all possible processes. Since the diode quality factor, *A*, appears in the denominator of the exponential in eq 6, at sufficiently large potentials a process with a smaller value of *A* can dominate the total interfacial flux even if the exchange current density, J_0, is larger for other parallel kinetic processes having larger *A* values.
(30) The cell potential was 20 mV vs MSCE, nearly 200 mV more negative than that of the $Me_2Fc^{+/0}$ system, but the built-in voltage was only 150 mV smaller for the n-InP/CH_3OH−THF−$Me_{10}Fc^{+/0}$ contact than for the n-InP/CH_3OH−$Me_2Fc^{+/0}$ contact. This is likely due to the slight difference in the apparent band edge positions between the two different solvent systems that were required for these measurements.
(31) Yang, E. S.; Chan, M.; Wahl, A. C. *J. Phys. Chem.* **1975**, *79*, 2049.
(32) Dai, S. Thesis, University of Tennessee, 1990.
(33) Nielson, R. M.; McManis, G. E.; Safford, L. K.; Weaver, M. J. *J. Phys. Chem.* **1989**, *93*, 2152. In this work, the self-exchange rate constant, k_{se}, for $Me_{10}Fc^{+/0}$ was not reported in methanol. However, k_{se} for $Fc^{+/0}$ was reported in methanol as well as in some solvents for which k_{se} for $Me_{10}Fc^{+/0}$ was also reported. In most cases, k_{se} of $Me_{10}Fc^{+/0}$ exceeded that of $Fc^{+/0}$ by approximately a factor of 3. To arrive at a reorganization energy for $Me_{10}Fc^{+/0}$ in methanol, k_{se} of $Fc^{+/0}$ in methanol was multiplied by 3 and converted to a reorganization energy by the equation: $k_{se} = Z_{bi}\, e^{-(\lambda/4kT)}$ where $Z_{bi} \approx 10^{11}$ M^{-1} s^{-1} is the collisional frequency for bimolecular reactions at room temperature, as given in: Marcus, R. A. *J. Phys. Chem.* **1963**, *67*, 853.
(34) Nagasubramanian, G.; Wheeler, B. L.; Bard, A. J. *J. Electrochem. Soc.* **1983**, *130*, 1680.
(35) Mead, C. A.; Spitzer, W. G. *Phys. Rev.* **1964**, *134*, A713.
(36) Newman, N.; Kendelewicz, T.; Bowman, L.; Spicer, W. E. *Appl. Phys. Lett.* **1985**, *46*, 1176.
(37) Ibach, H.; Luth, H. *Solid-State Physics*; Springer-Verlag: Berlin, 1990.